Article

Chemical Synthesis and Characterization of Pd/SiO$_2$: The Effect of Chemical Reagent

Aram L. Bugaev * , **Vladimir A. Polyakov, Andrei A. Tereshchenko** , **Ashura N. Isaeva,**
Alina A. Skorynina , **Elizaveta G. Kamyshova** , **Andriy P. Budnyk, Tatiana A. Lastovina ***
and Alexander V. Soldatov

The Smart Materials Research Center, Southern Federal University, 178/24 Sladkova,
Rostov-on-Don 344090, Russia; v.polakov93@gmail.com (V.A.P.); tereshch1@yandex.ru (A.A.T.);
isaeva.ashura@yandex.ru (A.N.I.); alinaskorynina@rambler.ru (A.A.S.); kamyshova.liza@gmail.com (E.G.K.);
abudnik.sfedu@yandex.ru (A.P.B.); soldatov@sfedu.ru (A.V.S.)
* Correspondence: abugaev@sfedu.ru (A.L.B.); lastovina.t@yandex.ru (T.A.L.);
  Tel.: +7-863-305-1996 (A.L.B. & T.A.L.)

Abstract: The size and shape distribution of metal nanoparticles (NPs) are important parameters that need to be tuned in order to achieve desired properties of materials for practical applications. In the current work, we present the synthesis of palladium NPs supported on silica by three different methods, applying reduction by sodium borohydride, hydrazine vapors, and polyethylene glycol (PEG). The synthesized materials were characterized by X-ray diffraction, X-ray fluorescence, transmission electron microscopy, surface area and porosity measurements, and thermogravimetric analysis. Similar nanoparticle sizes with narrow size distribution centered at 8 nm were obtained after reduction by sodium borohydride and hydrazine vapors, whereas the smallest particle size of about 4.8 nm was obtained after reduction by PEG. The effect of modification of the initial palladium chloride compound by ammonium hydroxide was found to lead to the formation of larger particles with average size of 15 nm and broader size distribution. In addition, the process of the reduction of palladium by PEG at different reduction stages was monitored by UV-Vis spectroscopy. CO-stripping voltammetry showed that reduction in hydrazine and in PEG allowed the preparation of Pd NPs with high electrochemically-active surface area. Such NPs are promising materials for electrocatalysis.

1. Introduction

Noble metal nanoparticles (NPs) find numerous applications in catalysis [1–4], electrochemistry [5], biology [6,7], medicine [8,9], and other fields. In particular, palladium is one of the best-performing metal catalysts for selective hydrogenation of alkynes [10–14]. Numerous studies focus on the size- and shape- dependent properties of palladium NPs [15–19], indicating that controlling the size and shape distribution of NPs during synthesis is an important step in designing functional materials with the required parameters for practical applications.

There are many effective ways to synthesize palladium NPs. As a general procedure, porous support such as amorphous carbons [20–25], alumina, silica, or other mesoporous oxides [19,26–29] is precipitated by palladium precursor containing palladium in its ionic phase [30] with subsequent reduction to Pd^0 and formation of palladium NPs [31]. Size and shape distributions of the resulting NPs depend on different parameters, such as type of support [32], temperature, and duration of reduction [33]. The role of the reducing agent has also been studied [34]. In particular, reduction in H$_2$ atmosphere can lead to the formation of particles 1 to 10 nm in size [30,33]. Another approach is to

use a reducing agent in liquid form. For example, 2 nm palladium particles on polymeric supports were obtained by reduction in sodium borohydride [35]. Having shown good reducing properties, hydrazine was used to synthesize palladium [36] and nickel NPs [37] in liquid phase. The obtained NPs were 4–8 nm in the case of palladium, and 9 nm for nickel.

In the current work, the traditional synthesis of silica-supported palladium NPs applying reduction of palladium precursor in hydrazine or sodium borohydride was compared with the solvothermal polyol synthesis. Detailed characterization of the synthesized materials was performed using X-ray powder diffraction (XRPD), X-ray fluorescence (XRF), transmission electron microscopy (TEM), surface area and porosity measurements, and thermogravimetric analysis (TGA). The effect of modifying the initial palladium chloride compound with ammonium hydroxide was studied. The process of the reduction of palladium in polyethylene glycol (PEG) was monitored by UV-Vis spectroscopy, which allowed observation of the time-evolution of nanoparticle formation. CO-stripping voltammetry showed that NPs obtained via reduction in hydrazine using ammonia complex of the palladium salt and in PEG had high electrochemical surface area (ECSA), which makes them promising materials for electrocatalysis.

2. Materials and Methods

2.1. Synthesis of Supported Palladium NPs

At the first step of the synthesis, 0.05 g of palladium chloride (Alfa Aesar, Haverhill, MA, USA, 99.999%) was dissolved in hydrochloric acid (Sigma Tec, Moscow, Russia, 99.99%), and 0.136 g of silica substrate (Aldrich, St. Louis, MA, USA, 5–15 nm, 99.5%) was precipitated by the resulting solution. Palladium chloride concentration in the solution was calculated to obtain the final concentration of Pd 18% *w/w*. The obtained SiO_2-supported complex was dried for 48 h at 60 °C. The reaction efficiency was 99%. Then, the SiO_2-supported palladium complex was used to prepare the palladium NPs using sodium borohydride, hydrazine, and polyethylene glycol-200 (Alfa Aesar, Haverhill, MA, USA, 99%) as reduction agents.

During the first synthesis, SiO_2-supported palladium complex was mixed with 1:5 solution of ethylene glycol (Alfa Aesar, Haverhill, MA, USA, 99%) in water. The mixture was treated in an ultrasonic bath for 5 min with subsequent stirring for 10 min. Then, a double excess of 1 M sodium borohydride (Alfa Aesar, Haverhill, MA, USA, 98%) water solution was added, and the resulting mixture was stirred for another 40 min. At the final stage of the synthesis, the obtained suspension was filtered, washed with deionized water, and dried. Because this sample was synthesized using $NaBH_4$ as a reducing agent, we will refer to it as Pd-NPs$_{NaBH_4}$. The calculated reaction efficiency was 99%.

For the synthesis with hydrazine as reduction agent, SiO_2-supported palladium complex was mixed with ethanol, and then was stuck to a lab watch glass. The sample was then reduced for 15 min in the vapors of hydrazine (Alfa Aesar, Haverhill, MA, USA, 98 + %) heated to 80 °C. During this procedure, a noticeable change in the color of the sample from orange to black was clearly observed. This sample will be referred to as Pd-NPs$_{hydrazine}$. The reaction efficiency was 61%. Some of the SiO_2-supported complex was subjected to the same procedure as described above for Pd-NPs$_{hydrazine}$, using ammonium hydroxide (Alfa Aesar, Haverhill, MA, USA, 28–30%) solution instead of ethanol. We will refer to this sample as Pd-NPs$_{ammonia,hydrazine}$. Both samples reduced in hydrazine vapors were washed with distilled water and centrifuged at 12,000 rpm three times, 15 min each, and then dried. The reaction efficiency in this case was 58%.

Finally, SiO_2-supported palladium complex was used for the solvothermal polyol synthesis of the SiO_2-supported palladium NPs. For this purpose, the SiO_2-supported complex was dispersed in 60 mL PEG and placed in a high-pressure reactor BR-200 (Berghof, Eningen, Germany). The prepared suspension was heated under stirring to 180 °C and held for 2 h. The aliquots of the reaction mixture at different time intervals (i.e., at the start and after 15, 30, 45, 60, 90, 120 min at 180 °C and after cooling)

were extracted for UV-Vis measurements (vide infra). After cooling, the prepared powder was washed with distilled water and dried. The reaction efficiency was 64%.

2.2. X-ray Fluorescence Spectroscopy

XRF spectroscopy was used to obtain information about the elemental composition and Pd loading on SiO_2. We carried out measurements using an M4 Tornado spectrometer (Bruker, Billerica, MA, USA) with an XFlash 430 detector in the range from 0 to 25 keV. The measurements were made at three different points of each sample. Then, the average Pd content was calculated for each sample and compared to the theoretical Pd loading on SiO_2.

2.3. Transmission Electron Microscopy

TEM was used to determine the size distribution of the synthesized samples. TEM micrographs were collected using an FEI Tecnai G2 Spirit TWIN transmission electron microscope operated at an accelerating voltage of 80 kV. The images from TEM were processed in ImageJ (Version 1.50i, National Institutes of Health, Bethesda, MD, USA) code [38].

2.4. X-ray Powder Diffraction

We carried out XRPD measurements using a D2 PHASER (Bruker, Billerica, MA, USA) diffractometer in Bragg–Brentano geometry. The experimental data were collected in the 2θ range from 10–100° using Cu K_α radiation with a step of 0.01° and acquisition time of 0.5 s. Corundum sample was measured under the same conditions to determine the instrumental contribution to the peaks broadening. To obtain structural parameters, Rietveld refinement procedure [39] was applied to the experimental diffraction patterns using Jana2006 (Version 25/10/2015, Institute of Physics CAS, Prague, Czech Republic) code [40]. The pseudo-Voight functions were used to describe the shape of the Bragg peaks. The 2θ range from 10–34° was excluded from the analysis, as it contained only the characteristic broad peak originating from the amorphous silica support and the background from the PMMA cuvette used for the measurements. Then, we applied a Williamson–Hall analysis to the fitted data to determine the contributions from microstrains and particle size.

2.5. UV-Vis Spectroscopy

The formation of Pd NPs in PEG during two hours of synthesis was monitored by UV-Vis spectroscopy with a UV-2600 spectrophotometer (Shimadzu, Kyoto, Japan). The aliquots of the reaction mixture at different time intervals (i.e., at start and after 15, 30, 45, 60, 90, 120 min at 180 °C and after cooling) were extracted. The aliquots were cooled down to room temperature and measured in a standard 2 mm quartz Suprasil cuvette against the ethylene glycol reference with 2 nm step in transmittance.

2.6. Specific Surface Area and Porosity Measurements

The Brunauer–Emmett–Teller (BET) and Langmuir models specific surface area (SSA) were calculated from the nitrogen adsorption/desorption isotherms recorded at 77 K using ASAP 2020 (Micromeritics) analyzer. Prior to the N_2 measurements, Pd/SiO_2 samples were degassed at 250 °C for 12 h. The pore size distributions were calculated from the desorption branches of the isotherms using the Barrett–Joyner–Halenda (BJH) [41] model and the density functional theory (DFT) model.

2.7. Thermogravimetric Analysis

The thermogravimetric analysis (TGA) was carried out by STA 449 F5 (Netzsch, Selb, Germany) in the air atmosphere with the heating rate of 10 °C/min. The results of TGA are reported in Section S2 of the Supplementary Materials.

2.8. CO-Stripping Voltammetry

　　CO-stripping cyclic voltammetry (CV) was used to determine the electrochemical surface area of the Pd/SiO_2. For the preparation of catalytic inks, 4 mg of the sample was mixed with 514 μL of isopropanol and 57 μL of 0.5% Nafion solution and deposited after sonication and stirring onto the surface of the glassy carbon electrode. The electrochemical measurements in the three-electrode cell were performed in 0.1 M $HClO_4$ with the platinum counter electrode and Ag/AgCl (sat. KCl solution) reference electrode. All potentials in this study are referred to the reversible hydrogen electrode (RHE).

　　Before the CO-stripping experiment, the solution was purged by bubbling Ar for 30 min. Then, 10 cycles in the potential range from 0.1 to 1.33 V (vs. RHE) were recorded at a scan rate of 50 mV/s. The CO stripping voltammograms were recorded after saturation of the solution by CO at the constant potential $E = 0.15$ V vs. RHE, followed by 40 min Ar bubbling under the same conditions. After this, three voltammograms were recorded. All measurements were performed at room temperature.

3. Results and Discussion

3.1. Structure and Morphology of Pd/SiO₂

　　The size distributions of the samples shown in Figure 1 were obtained by counting 700–900 NPs for each sample. Similar size distributions centered around 8 nm were obtained for the sample reduced by sodium borohydride, Pd-NPs$_{NaBH_4}$, and the sample reduced in the vapor of hydrazine Pd-NPs$_{hydrazine}$. However, the latter includes particle agglomerates with sizes from 15 to 35 nm. In both cases, palladium NPs had spherical or close to spherical shape. For the sample reduced in vapors of hydrazine in the presence of ammonium hydroxide (Pd-NPs$_{ammonia,hydrazine}$), larger particles around 15 nm with broad size distribution were obtained. The quantitative results of TEM size distribution analysis for these three samples are summarized in Table 1.
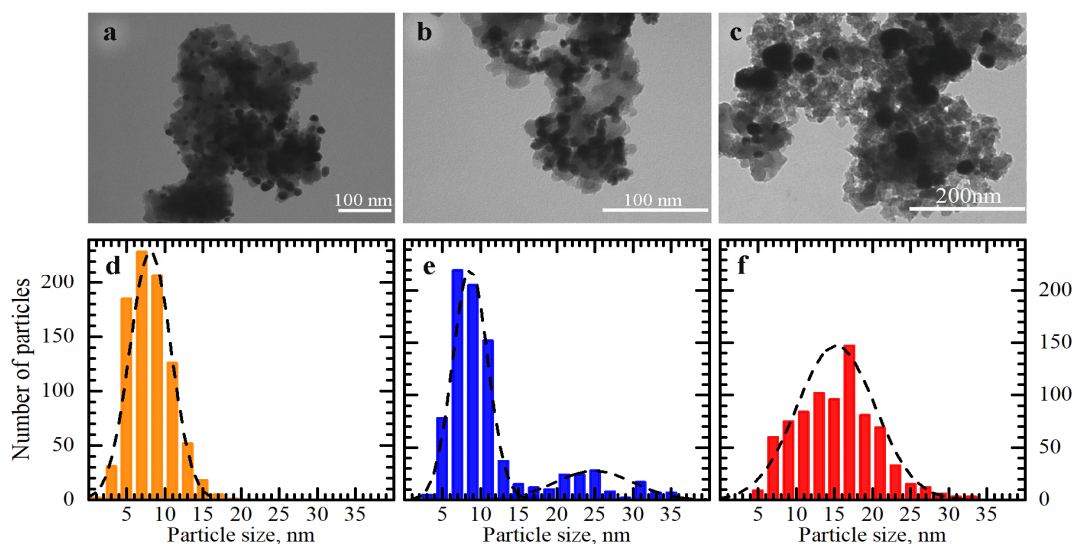

Figure 1. Representative TEM micrographs with corresponding particle size distributions for Pd/SiO₂ samples reduced by NaBH₄: (**a**) sample Pd-NPs$_{NaBH_4}$; reduced by hydrazine: samples (**b**) Pd-NPs$_{hydrazine}$ and (**c**) Pd-NPs$_{ammonia,hydrazine}$, with corresponding size distributions in parts (**d**–**f**). NP: nanoparticle.

Table 1. Average particle size D_{TEM} obtained by TEM with corresponding size distribution, average crystalline size D_{XRPD}, and lattice parameter a_{XRPD} by X-ray powder diffraction (XRPD), and Pd content ω_{XRF} in wt % determined by X-ray fluorescence (XRF).

Sample Name	$<D_{TEM}>$, nm	$<D_{XRPD}>$, nm	a_{XRPD}	ω_{XRF} Pd, wt %
Pd-NPs$_{NaBH_4}$	8.1 ± 2.7	6.0 (0.6)	3.907 ± 0.002	19.4
Pd-NPs$_{hydrazine}$	8.6 ± 2.3 and 24.9 ± 5.1	8.3 (0.6)	3.891 ± 0.001	11.1
Pd-NPs$_{ammonia,hydrazine}$	15.2 ± 5.1	13.7 (1.0)	3.893 ± 0.002	10.4
Pd-NPs$_{PEG}$	-	4.8 (1.2)	4.01 ± 0.01	11.6

When PEG was used as a reduction agent, the slow formation of the SiO$_2$ decorated with ultra-small palladium NPs was observed (Figure 2). It should be noted that 90 min after the start of the reaction, there were no significant changes in the morphology of the NPs. The small size of the obtained NPs and their dense loading inside the silica pores prevented us from performing quantitative TEM size distribution analysis for this sample.
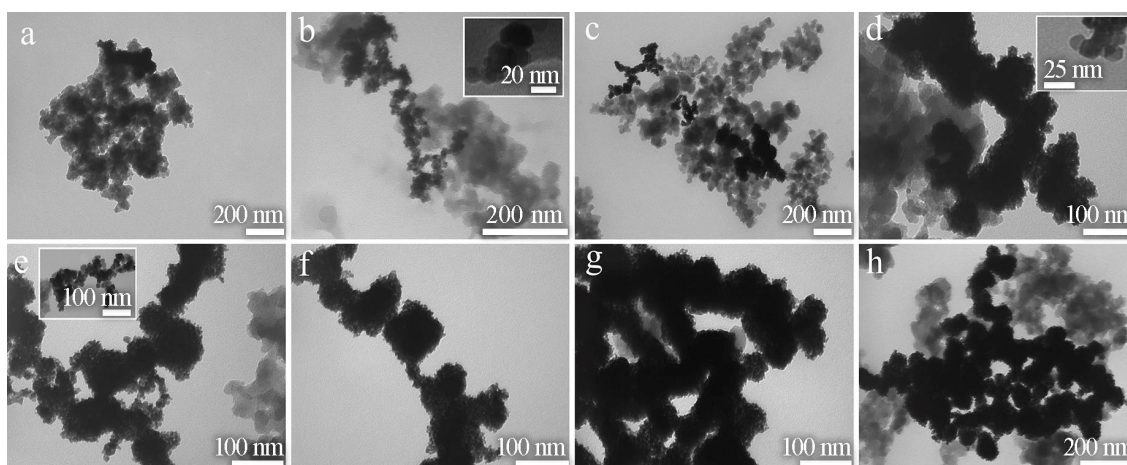

Figure 2. Representative TEM micrographs for Pd/SiO$_2$ samples reduced by polyethylene glycol (PEG) at different time intervals after reaching 180 °C: (**a**) 0 min; (**b**) 15 min; (**c**) 30 min; (**d**) 45 min; (**e**) 60 min; (**f**) 90 min; (**g**) 120 min; and (**h**) 120 min, after cooling.

XRPD analysis (Figure 3) confirmed the formation of the particles with *fcc* structure for all the samples, which is in good agreement with the results frequently reported for nanostructured palladium samples [16,42]. During the refinement, we obtained the following lattice parameters: 3.907, 3.891, 3.893, and 4.01 Å for Pd-NPs$_{NaBH_4}$, Pd-NPs$_{hydrazine}$, Pd-NPs$_{ammonia,hydrazine}$, and Pd-NPs$_{PEG}$, respectively (see Table 1 for the error bars). These lattice parameters are also close to those reported for palladium NPs and bulk palladium materials [12,17,24,30,33]. According to the analysis of peaks broadening, the mean crystallite size was 6.1 nm in the case of palladium reduced by NaBH$_4$, and in case of reduction by hydrazine using ethanol and ammonia, the crystallite sizes were 8.4 nm and 13.7 nm, respectively, which is reported in Table 1 together with TEM results. The fact that the average particle size of Pd-NPs$_{hydrazine}$ was close to 8 nm proves that the bigger fraction of particles—shown in Figure 1b—does not actually originate from big (15–35 nm) particles, but contains agglomerates of smaller ones with average size close to 8 nm. For Pd-NPs$_{ammonia,hydrazine}$, the XRPD results were in good agreement with the particle size determined by TEM, indicating that in the case of ammonia the resulting size of the NPs was larger. This is explained by the fact that ammonia modifies the initial [PdCl$_4$]$^{2-}$ compound into [Pd(NH$_3$)$_4$]$^{2+}$, which has lower redox potential (see Section S1 of the Supplementary Materials). In agreement with TEM data, the smallest particle size of 4.8 ± 1.2 nm was obtained for Pd-NPs$_{PEG}$. The higher error in determining this value originates from very weak

(220) and (311) reflections, which complicates the analysis. According to XRF analysis, Pd-NPs$_{NaBH_4}$ and Pd-NPs$_{PEG}$ samples contained 19.4 and 11.6 wt % of palladium, respectively, which is close to the expected value according to the loading of the initial chemicals. For the samples reduced in hydrazine vapors, the experimental values of palladium content were lower than the theoretical ones. This indicates a partial loss of non-reduced Pd species during the synthesis.

As shown in Figure 4a, the nitrogen adsorption–desorption isotherms of the SiO$_2$ and Pd/SiO$_2$ particles are of type IV based on the IUPAC classification, with H3 hysteresis loop at $p/p_0 > 0.8$. The increment of adsorption at $p/p_0 = 1.0$ was caused by larger mesopores that may be accompanied with slit-shaped pores [43]. The increase in the SSA values was observed for all samples, but only Pd-NPs$_{PEG}$ had substantially low ones (Table 2). For the pristine SiO$_2$ particles, a multitude of pore types (macropores, mesopores, micropores, and ultramicropores) was observed (Figure 4b,c). After impregnation of the SiO$_2$ with the palladium complex and its further reduction by NaBH$_4$ and hydrazine, all types of pores were preserved, their quantity being lowered. The use of NaBH$_4$ led to a larger quantity of macropores in the resulting material, whereas the samples of Pd/SiO$_2$ obtained by the reduction in hydrazine possessed the same quantity of macro- and mesopores. The high SSA value of the Pd-NPs$_{NaBH_4}$ sample means that macropores more evidently contributed to SSA. Pd-NPs$_{PEG}$ was found to contain only mesopores. This indicates a predominant formation of the Pd NPs inside micropores and mesopores, resulting in smaller NPs.
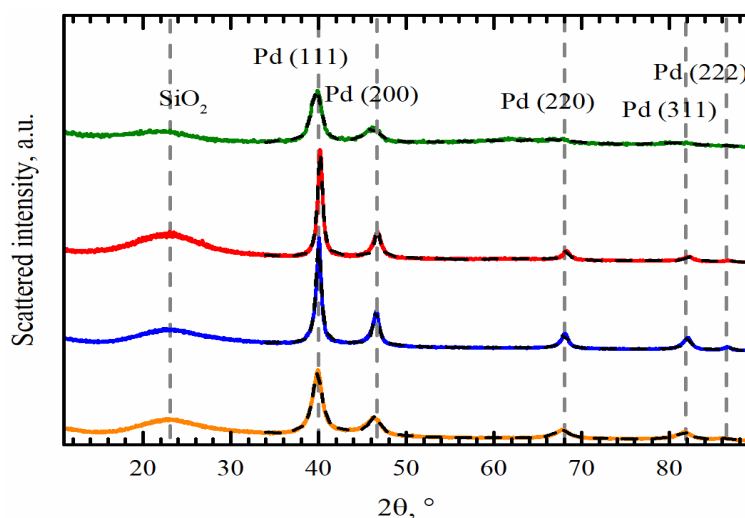

Figure 3. Experimental (solid colored lines) and theoretical (dashed black lines) diffraction patterns for Pd/SiO$_2$ samples reduced in NaBH$_4$ (**orange**); in hydrazine (**blue**); in hydrazine with ammonia (**red**); and in PEG (**green**). Dashed vertical lines highlight the positions of Pd Bragg reflections and SiO$_2$ reflection.

Table 2. Specific surface area (SSA) for the synthesized Pd/SiO$_2$ NPs and SiO$_2$ support. BET: Brunauer–Emmett–Teller.

| Sample Name	SSA, m^2/g	
	BET	Langmuir
Pd-NPs$_{NaBH_4}$	343	418
Pd-NPs$_{hydrazine}$	298	366
Pd-NPs$_{ammonia,hydrazine}$	290	355
Pd-NPs$_{PEG}$	27	34
SiO$_2$	482	587
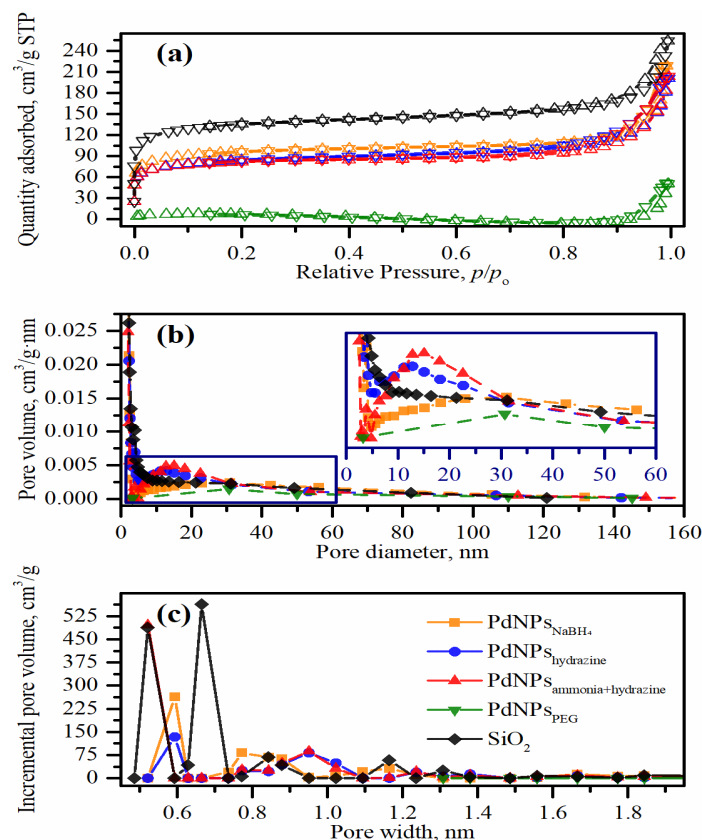
Figure 4. (**a**) N_2 sorption isotherms for the samples: Pd-NPs$_{NaBH_4}$ (orange), Pd-NPs$_{hydrazine}$ (blue), Pd-NPs$_{ammonia,hydrazine}$ (red), Pd-NPs$_{PEG}$ (green), and SiO_2 support (black). Absorption and desorption directions are marked by up- and down-triangles, respectively. Corresponding Barrett–Joyner–Halenda (BJH) and density functional theory (DFT) pore size distributions are shown in parts (**b**) and (**c**), respectively.

3.2. The Process of Nanoparticle Growth in PEG

The synthesis of Pd-NPs$_{PEG}$ sample was monitored ex situ (at room temperature) by attenuated total reflectance (ATR) Fourier transform infrared spectroscopy (FTIR) and UV-Vis spectroscopy in transmittance (Figure 5, parts (a) and (b), respectively). The starting spectra of the mixture of the reagents heated to 180 °C are shown in black, the final ones are in green. The FTIR spectra (Figure 5a) are essentially those of PEG with no appreciable changes during a two-hour reaction run. Instead, the sequence of UV-Vis spectra (Figure 5b) with intermediates taken after 15, 30, 45, 60, and 90 min of reaction shows an increase in absorption along the reaction run, which is the evidence of the formation of Pd NPs. In particular, there is a clearly observable band at 325 nm indicative of Pd^{II} species (together with a less visible one at 440 nm) [44]. This band was consumed during the synthesis, and the final curve profile exhibits a broad absorption across the ultraviolet-visible range, which is characteristic of the reduced palladium [45]. This is highlighted by the inset, where the final curve is shown in absorbance values as a function of photon energy.
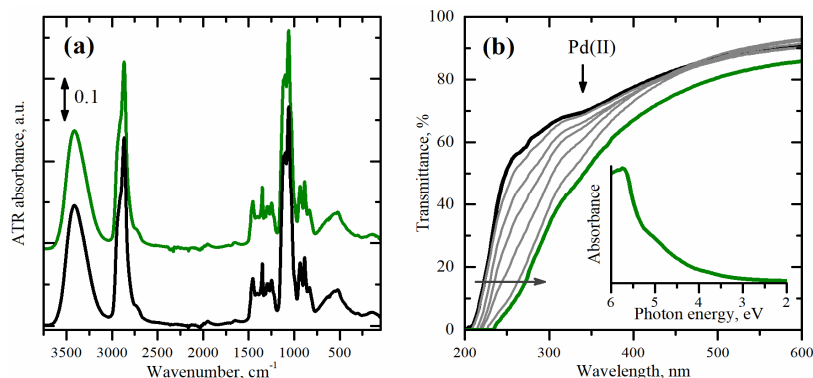
Figure 5. (**a**) Fourier transform infrared (FTIR) and (**b**) UV-Vis spectra of the mixture of reagents for Pd-NPs$_{PEG}$ collected at the beginning (black) and at the end (green) of the synthesis. Intermediates are shown in grey. ATR: attenuated total reflectance.

3.3. Electrocatalytic Properties of Pd/SiO$_2$

The ECSA values of all prepared catalysts were calculated to get insight into available active sites at the surface of the catalysts. The CO-stripping CV was used to determine the ECSA of the Pd NPs using the following equation [46]:

$$\text{ECSA} = \frac{Q}{G \cdot 420}, \tag{1}$$

where Q is the columbic charge (μC) for the CO$_{ads}$ oxidation, the columbic charge required to complete CO monolayer oxidation at the Pd surface is equal to 420 μC·cm^{-2} (the same as for Pt surfaces) [47], and G is the Pd loading (g) on the working electrode [48]. According to CO-stripping data, the peak around 1.1 V (vs. RHE) for Pd/SiO$_2$ samples corresponds to the oxidation of a CO monolayer. The CV curves showed only a single oxidation peak (Figure 6), whereas no CO oxidation was observed in the second CV curve, confirming the full removal of the CO$_{ads}$. The calculated ECSA of the Pd/SiO$_2$ catalysts can be arranged as follows: Pd-NPs$_{ammonia,hydrazine}$ (15.9 m^2 g^{-1}) > Pd-NPs$_{hydrazine}$ (11.1 m^2 g^{-1}) ≈ Pd-NPs$_{PEG}$ (10.7 m^2 g^{-1}) > Pd-NPs$_{NaBH_4}$ (1.8 m^2 g^{-1}). The onset potentials of CO oxidation starting from 0.954 V were shifted to 1 V for the Pd-NPs$_{ammonia,hydrazine}$.
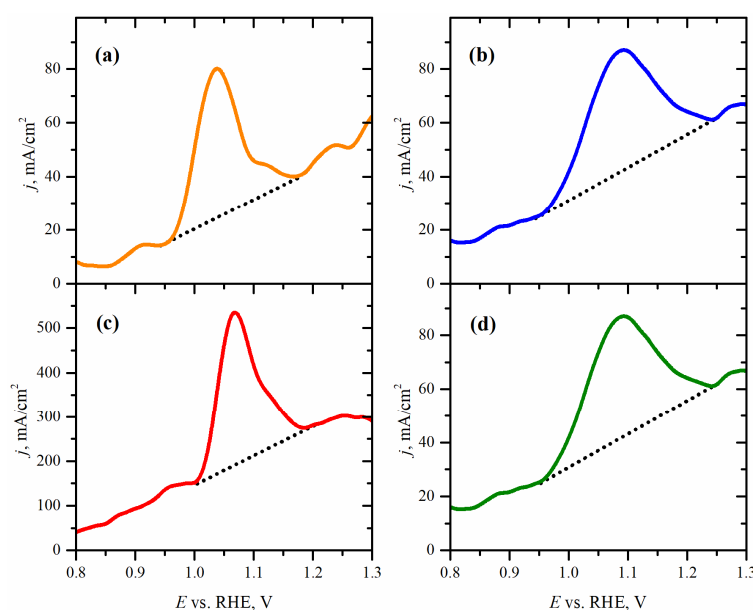
Figure 6. CO-stripping of (**a**) Pd/SiO$_2$ samples reduced in NaBH$_4$; in hydrazine: (**b**) Pd-NPs$_{hydrazine}$ and (**c**) Pd-NPs$_{ammonia,hydrazine}$; and (**d**) Pd-NPs$_{PEG}$ collected at 25 °C in 0.1 M HClO$_4$ solution.

No electrochemical peaks for the CO oxidation were found in the second and third cycles, indicating the formation of a CO monolayer and its full conversion. It can be seen that the reduction both in hydrazine using ammonia complex of the palladium salt and in PEG allows one to prepare Pd NPs with high ECSA. Therefore, such materials are likely to be widely applied in electrocatalysis.

4. Conclusions

We have presented the synthesis of supported palladium NPs using different reduction agents: hydrazine, borohydride, and PEG. It was found that by varying the synthesis parameters it was possible to prepare Pd NPs with sizes from 4.8 to 14 nm. The use of PEG resulted in the formation of ultra-small Pd NPs. All the samples were electrochemically active with high CO tolerance. The synthesis procedures can be easily adopted for the production of different noble metal NPs. In addition, we have studied the effect of modification of the initial $[PdCl_4]^{2-}$ to $[Pd(NH_3)_4]^{2+}$ by ammonium hydroxide, which led to the formation of larger particles. The smallest particle size of 4.8 nm was obtained after PEG reduction. Moreover, the process of palladium reduction in PEG was monitored by UV-Vis spectroscopy, allowing observation of the time-evolution of nanoparticle formation. Applying CO-stripping voltammetry, we showed that the reduction of palladium both in hydrazine using ammonia complex of the palladium salt and in PEG made it possible to obtain Pd NPs with high ECSA, which makes them promising materials for electrocatalytic applications.

References

1. Hegedűs, L.; Máthé, T. Selective heterogeneous catalytic hydrogenation of nitriles to primary amines in liquid phase. *Appl. Catal. A* **2005**, *296*, 209–215. [CrossRef]
2. Lee, C.S.; Lee, J.H.; Kang, B.K.; Kim, J.S.; Kim, G.J.; Koh, K.; Koh, S.-K. High Catalytic Performance of Uniformly Loaded Pd Nanoparticles on Activated Carbon through the Nanoparticles on Powder Process. *J. Nanosci. Nanotechnol.* **2016**, *16*, 12037–12041. [CrossRef]
3. Omar, S.; Abu-Reziq, R. Palladium Nanoparticles Supported on Magnetic Organic-Silica Hybrid Nanoparticles. *J. Phys. Chem. C* **2014**, *118*, 30045–30056. [CrossRef]
4. Bugaev, A.L.; Usoltsev, O.A.; Lazzarini, A.; Lomachenko, K.A.; Guda, A.A.; Pellegrini, R.; Carosso, M.; Vitillo, J.G.; Groppo, E.; van Bokhoven, J.; et al. Time-resolved operando studies of carbon supported Pd nanoparticles under hydrogenation reactions by X-ray diffraction and absorption. *Faraday Discuss.* **2018**. [CrossRef]
5. Murray, R.W. Nanoelectrochemistry: Metal nanoparticles, nanoelectrodes, and nanopores. *Chem. Rev.* **2008**, *108*, 2688–2720. [CrossRef] [PubMed]
6. Hu, M.; Chen, J.Y.; Li, Z.Y.; Au, L.; Hartland, G.V.; Li, X.D.; Marquez, M.; Xia, Y.N. Gold nanostructures: Engineering their plasmonic properties for biomedical applications. *Chem. Soc. Rev.* **2006**, *35*, 1084–1094. [CrossRef] [PubMed]
7. Anker, J.N.; Hall, W.P.; Lyandres, O.; Shah, N.C.; Zhao, J.; Van Duyne, R.P. Biosensing with plasmonic nanosensors. *Nat. Mater.* **2008**, *7*, 442–453. [CrossRef] [PubMed]

8.	El-Sayed, I.H.; Huang, X.H.; El-Sayed, M.A. Surface plasmon resonance scattering and absorption of anti-EGFR antibody conjugated gold nanoparticles in cancer diagnostics: Applications in oral cancer. *Nano Lett.* **2005**, *5*, 829–834. [CrossRef] [PubMed]

9.	Lal, S.; Clare, S.E.; Halas, N.J. Nanoshell-enabled photothermal cancer therapy: Impending clinical impact. *Accounts Chem. Res.* **2008**, *41*, 1842–1851. [CrossRef] [PubMed]

10.	Borodziński, A.; Bond, G.C. Selective hydrogenation of ethyne in ethene-rich streams on palladium catalysts. Part 1. Effect of changes to the catalyst during reaction. *Catal. Rev.* **2006**, *48*, 91–144. [CrossRef]

11.	Borodziński, A.; Bond, G.C. Selective hydrogenation of ethyne in ethene-rich streams on palladium catalysts, Part 2: Steady-state kinetics and effects of palladium particle size, carbon monoxide, and promoters. *Catal. Rev.* **2008**, *50*, 379–469. [CrossRef]

12.	Bugaev, A.L.; Guda, A.A.; Lazzarini, A.; Lomachenko, K.A.; Groppo, E.; Pellegrini, R.; Piovano, A.; Emerich, H.; Soldatov, A.V.; Bugaev, L.A.; et al. In situ formation of hydrides and carbides in palladium catalyst: When XANES is better than EXAFS and XRD. *Catal. Today* **2017**, *283*, 119–126. [CrossRef]

13.	Tew, M.W.; Janousch, M.; Huthwelker, T.; van Bokhoven, J.A. The roles of carbide and hydride in oxide-supported palladium nanoparticles for alkyne hydrogenation. *J. Catal.* **2011**, *283*, 45–54. [CrossRef]

14.	Tew, M.W.; Nachtegaal, M.; Janousch, M.; Huthwelker, T.; van Bokhoven, J.A. The irreversible formation of palladium carbide during hydrogenation of 1-pentyne over silica-supported palladium nanoparticles: In situ Pd K and L_3 edge XAS. *Phys. Chem. Chem. Phys.* **2012**, *14*, 5761–5768. [CrossRef] [PubMed]

15.	Newton, M.A.; Belver-Coldeira, C.; Martinez-Arias, A.; Fernandez-Garcia, M. Dynamic in situ observation of rapid size and shape change of supported Pd nanoparticles during CO/NO cycling. *Nat. Mater.* **2007**, *6*, 528–532. [CrossRef] [PubMed]

16.	Zlotea, C.; Cuevas, F.; Paul-Boncour, V.; Leroy, E.; Dibandjo, P.; Gadiou, R.; Vix-Guterl, C.; Latroche, M. Size-dependent hydrogen sorption in ultrasmall Pd clusters embedded in a mesoporous carbon template. *J. Am. Chem. Soc.* **2010**, *132*, 7720–7729. [CrossRef] [PubMed]

17.	Berube, V.; Radtke, G.; Dresselhaus, M.; Chen, G. Size effects on the hydrogen storage properties of nanostructured metal hydrides: A review. *Int. J. Energy Res.* **2007**, *31*, 637–663. [CrossRef]

18.	Langhammer, C.; Zhdanov, V.P.; Zoric, I.; Kasemo, B. Size-dependent hysteresis in the formation and decomposition of hydride in metal nanoparticles. *Chem. Phys. Lett.* **2010**, *488*, 62–66. [CrossRef]

19.	Borodziński, A. The effect of palladium particle size on the kinetics of hydrogenation of acetylene-ethylene mixtures over Pd/SiO2 catalysts. *Catal. Lett.* **2001**, *71*, 169–175. [CrossRef]

20.	Xu, X.; Li, Y.; Gong, Y.T.; Zhang, P.F.; Li, H.R.; Wang, Y. Synthesis of palladium nanoparticles supported on mesoporous N-doped carbon and their catalytic ability for biofuel upgrade. *J. Am. Chem. Soc.* **2012**, *134*, 16987–16990. [CrossRef] [PubMed]

21.	Lei, Y.; Lu, J.; Luo, X.Y.; Wu, T.P.; Du, P.; Zhang, X.Y.; Ren, Y.; Wen, J.G.; Miller, D.J.; Miller, J.T.; et al. Synthesis of porous carbon supported palladium nanoparticle catalysts by atomic layer deposition: Application for rechargeable lithium-O2 battery. *Nano Lett.* **2013**, *13*, 4182–4189. [CrossRef] [PubMed]

22.	Agostini, G.; Lamberti, C.; Pellegrini, R.; Leofanti, G.; Giannici, F.; Longo, A.; Groppo, E. Effect of pre-reduction on the properties and the catalytic activity of Pd/carbon catalysts: A comparison with Pd/Al2O3. *ACS Catal.* **2014**, *4*, 187–194. [CrossRef]

23.	Piovano, A.; Lazzarini, A.; Pellegrini, R.; Leofanti, G.; Agostini, G.; Rudić, S.; Bugaev, A.L.; Lamberti, C.; Groppo, E. Progress in the characterization of the surface species in activated carbons by means of INS spectroscopy coupled with detailed DFT calculations. *Adv. Condens. Matter Phys.* **2015**, *2015*, 1–8. [CrossRef]

24.	Bugaev, A.L.; Guda, A.A.; Lomachenko, K.A.; Lazzarini, A.; Srabionyan, V.V.; Vitillo, J.G.; Piovano, A.; Groppo, E.; Bugaev, L.A.; Soldatov, A.V.; et al. Hydride phase formation in carbon supported palladium hydride nanoparticles by in situ EXAFS and XRD. *J. Phys. Conf. Ser.* **2016**, *712*. [CrossRef]

25.	Habibi, B.; Mohammadyari, S. Facile synthesis of Pd nanoparticles on nano carbon supports and their application as an electrocatalyst for oxidation of ethanol in alkaline media: The effect of support. *Int. J. Hydrog. Energy* **2015**, *40*, 10833–10846. [CrossRef]

26.	Groppo, E.; Agostini, G.; Piovano, A.; Muddada, N.B.; Leofanti, G.; Pellegrini, R.; Portale, G.; Longo, A.; Lamberti, C. Effect of reduction in liquid phase on the properties and the catalytic activity of Pd/Al2O3 catalysts. *J. Catal.* **2012**, *287*, 44–54. [CrossRef]

27. Bugaev, A.L.; Guda, A.A.; Lomachenko, K.A.; Srabionyan, V.V.; Bugaev, L.A.; Soldatov, A.V.; Lamberti, C.; Dmitriev, V.P.; van Bokhoven, J.A. Temperature- and pressure-dependent hydrogen concentration in supported PdH$_x$ nanoparticles by Pd K-edge X-ray absorption spectroscopy. *J. Phys. Chem. C* **2014**, *118*, 10416–10423. [CrossRef]

28. Bugaev, A.L.; Guda, A.A.; Lomachenko, K.A.; Bugaev, L.A.; Soldatov, A.V. Pd hydride and carbide studied by means of Pd K-edge X-ray absorption near-edge structure analysis. *Bull. Russ. Acad. Sci. Phys.* **2015**, *79*, 1180–1185. [CrossRef]

29. Ichikawa, Y.; Hioki, T.; Sugimoto, N.; Ichiki, A.; Motohiro, T. Hydrogen Storage Capacity of Pd Particles Dispersed in Mesoporous Silicas. *J. Nanosci. Nanotechnol.* **2016**, *16*, 12947–12951. [CrossRef]

30. Agostini, G.; Groppo, E.; Piovano, A.; Pellegrini, R.; Leofanti, G.; Lamberti, C. Preparation of supported Pd catalysts: From the Pd precursor solution to the deposited Pd^{2+} phase. *Langmuir* **2010**, *26*, 11204–11211. [CrossRef] [PubMed]

31. Geus, J.W.; van Dillen, A.J. Preparation of Supported Catalysts by Deposition-Precipitation. In *Handbook of Heterogeneous Catalysis*; Wiley-VCH Verlag GmbH & Co. KGaA: Weinheim, Germany, 2008.

32. Groppo, E.; Bertarione, S.; Rotunno, F.; Agostini, G.; Scarano, D.; Pellegrini, R.; Leofanti, G.; Zecchina, A.; Lamberti, C. Role of the Support in Determining the Vibrational Properties of Carbonyls Formed on Pd Supported on SiO$_2$-Al$_2$O$_3$, Al$_2$O$_3$, and MgO. *J. Phys. Chem. C* **2007**, *111*, 7021–7028. [CrossRef]

33. Tew, M.W.; Miller, J.T.; van Bokhoven, J.A. Particle size effect of hydride formation and surface hydrogen adsorption of nanosized palladium catalysts: L$_3$ edge vs. K edge X-ray absorption spectroscopy. *J. Phys. Chem. C* **2009**, *113*, 15140–15147. [CrossRef]

34. Groppo, E.; Agostini, G.; Borfecchia, E.; Wei, L.; Giannici, F.; Portale, G.; Longo, A.; Lamberti, C. Formation and Growth of Pd Nanoparticles Inside a Highly Cross-Linked Polystyrene Support: Role of the Reducing Agent. *J. Phys. Chem. C* **2014**, *118*, 8406–8415. [CrossRef]

35. Desforges, A.; Backov, R.; Deleuze, H.; Mondain-Monval, O. Generation of Palladium Nanoparticles within Macrocellular Polymeric Supports: Application to Heterogeneous Catalysis of the Suzuki-Miyaura Coupling Reaction. *Adv. Funct. Mater.* **2005**, *15*, 1689–1695. [CrossRef]

36. Wang, C.-C.; Chen, D.-H.; Huang, T.-C. Synthesis of palladium nanoparticles in water-in-oil microemulsions. *Colloids Surf. A Physicochem. Eng. Asp.* **2001**, *189*, 145–154. [CrossRef]

37. Wu, S.-H.; Chen, D.-H. Synthesis and characterization of nickel nanoparticles by hydrazine reduction in ethylene glycol. *J. Colloid Interface Sci.* **2003**, *259*, 282–286. [CrossRef]

38. Collins, T. ImageJ for microscopy. *Biotechniques* **2007**, *43*, S25–S30. [CrossRef]

39. Rietveld, H.M. A profile refinement method for nuclear and magnetic structures. *J. Appl. Crystallogr.* **1969**, *2*, 65–71. [CrossRef]

40. Petříček, V.; Dušek, M.; Palatinus, L. Crystallographic Computing System JANA2006: General features. *Z. Kristallogr.-Cryst. Mater.* **2014**, *229*, 345–352. [CrossRef]

41. Barrett, E.P.; Joyner, L.G.; Halenda, P.P. The Determination of Pore Volume and Area Distributions in Porous Substances. I. Computations from Nitrogen Isotherms. *J. Am. Chem. Soc.* **1951**, *73*, 373–380. [CrossRef]

42. Bugaev, A.L.; Guda, A.A.; Lomachenko, K.A.; Shapovalov, V.V.; Lazzarini, A.; Vitillo, J.G.; Bugaev, L.A.; Groppo, E.; Pellegrini, R.; Soldatov, A.V.; et al. Core-Shell Structure of Palladium Hydride Nanoparticles Revealed by Combined X-ray Absorption Spectroscopy and X-ray Diffraction. *J. Phys. Chem. C* **2017**, *121*, 18202–18213. [CrossRef]

43. Cui, J.; Sun, H.; Luo, Z.; Sun, J.; Wen, Z. Preparation of low surface area SiO$_2$ microsphere from wheat husk ash with a facile precipitation process. *Mater. Lett.* **2015**, *156*, 42–45. [CrossRef]

44. D'Souz, L.; Sampath, S. Preparation and Characterization of Silane-Stabilized, Highly Uniform, Nanobimetallic Pt—Pd Particles in Solid and Liquid Matrixes. *Langmuir* **2000**, *16*, 8510–8517. [CrossRef]

45. Creighton, J.A.; Eadon, D.G. Ultraviolet-visible absorption spectra of the colloidal metallic elements. *J. Chem. Soc. Faraday Trans.* **1991**, *87*, 3881–3891. [CrossRef]

46. Chen, D.; Cui, P.; He, H.; Liu, H.; Ye, F.; Yang, J. Carbon-supported hollow palladium nanoparticles with enhanced electrocatalytic performance. *RSC Adv.* **2015**, *5*, 10944–10950. [CrossRef]

47. Zadick, A.; Dubau, L.; Demirci, U.B.; Chatenet, M. Effects of Pd Nanoparticle Size and Solution Reducer Strength on Pd/C Electrocatalyst Stability in Alkaline Electrolyte. *J. Electrochem. Soc.* **2016**, *163*, F781–F787. [CrossRef]

48. Ding, L.G.; Yao, B.J.; Jiang, W.L.; Li, J.T.; Fu, Q.J.; Li, Y.A.; Liu, Z.H.; Ma, J.P.; Dong, Y.B. Bifunctional lmidazolium-Based Ionic Liquid Decorated UiO-67 Type MOF for Selective CO_2 Adsorption and Catalytic Property for CO_2 Cycloaddition with Epoxides. *Inorg. Chem.* **2017**, *56*, 2337–2344. [CrossRef] [PubMed]